

4 Result

4.1 Summary

To investigate the physical changes occurring in the Josephson junction based on the results of the previous sections, we used two methods to analyze the calculation result. The first involved examining the changes in the order parameter, $\cos \phi$. As a second method, we calculate the correlation function between the excited and ground states, and express it using an approximation formula for conductivity based on fluctuation-dissipation theory. Through analyzing the method of the order parameter, we revealed that the system exhibited an insulating state as the temperature decreased. Secondly, the approximation formula showed the following results. To evaluate the accuracy of the calculated results, we tested each section of the integration code by comparing it with the case without reservoir effects, comparing it with higher-order approximation methods, and checking for convergence depending on the calculation conditions.

4.2 Benchmark

Exact diagonalization in single mode

To compare with the result from exact diagonalization(ED), we set the condition when the bath has only a single mode. The result shows approximation method could be reliable in high temperatures ($\beta = 1$).

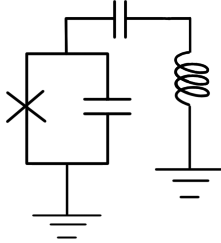


Figure 11: Brief circuit scheme for single bath condition. The crossing symbol refers to the insulated junction of Josephson junction.

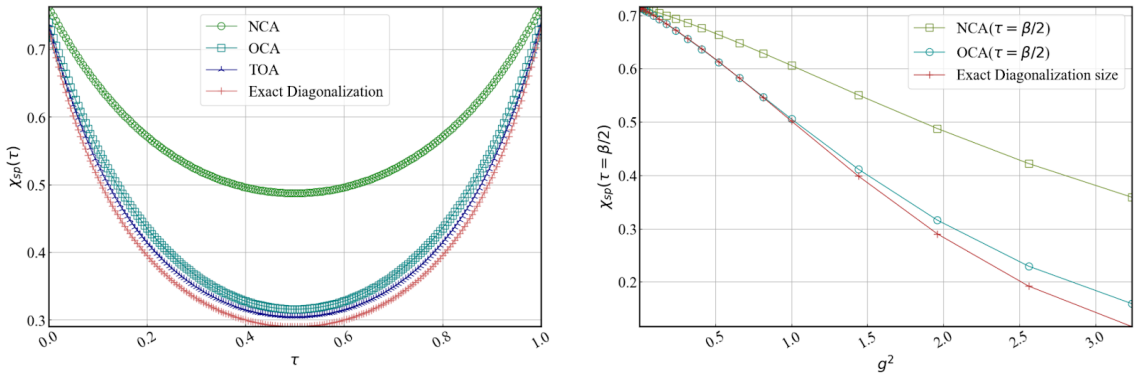


Figure 12: Result for single bath benchmark. For $\chi_{sp} - \tau$ (Left), it conducted on overall condition g (coupling strength with system-bath) = 1. With $\chi_{sp}(\tau = \beta/2) - g^2$ (Right), It shows that if order of perturbation increases, the results approach the exact results.

Multi-mode case

To investigate the convergence of the diagrammatic approximation method in a general bosonic reservoir condition, we calculated the order parameter and the correlation function using the NCA, OCA, and TOA. The results showed no significant difference between the OCA and TOA calculations, confirming that the OCA is a sufficiently convergent method.

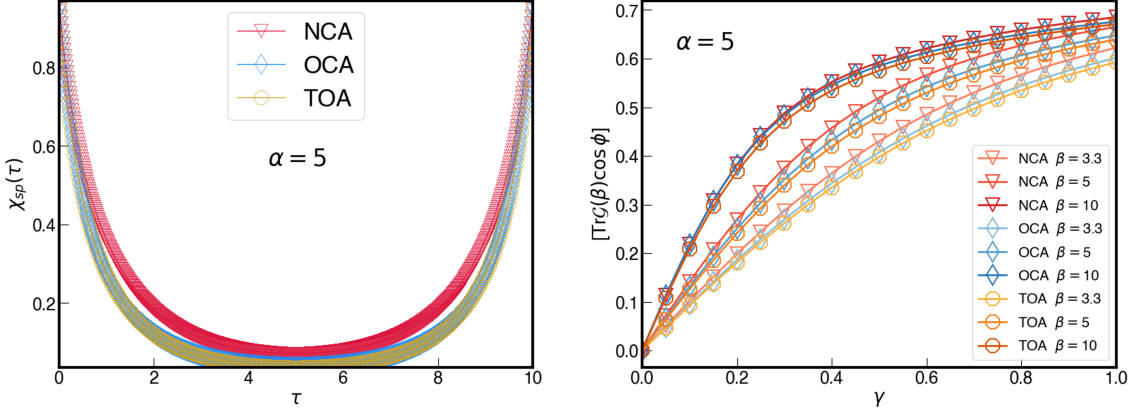


Figure 13: Calculation results of the order parameter and correlation function using each order of the approximation method. Both figures are for the case of $\alpha=5$, with the left figure showing temperatures between 0.3 and 0.1, the right figure is for the temperature condition of 0.1. It can be observed that the calculation results of OCA and TOA are converged. The size of the grid used for the calculation is 701.

Benchmarking solver code in $\alpha = 0$ condition

To check for the integration code, we compared the order parameter calculated using approximation methods for the case of $=0$ with the order parameter calculated using the state density matrix of the Josephson junction system. The results showed that the two cases were completely consistent.

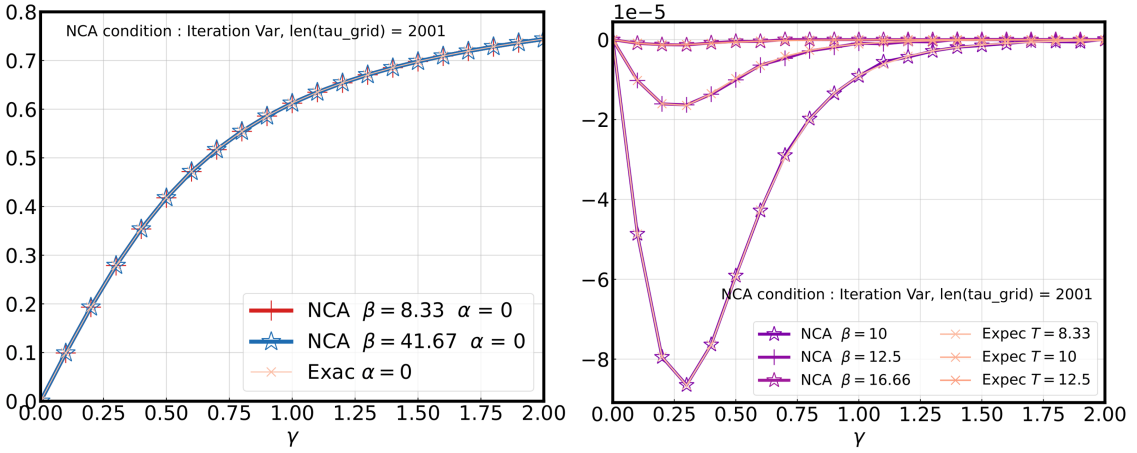


Figure 14: In the case of $\alpha = 0$, order parameter calculation using the approximation method should be consistent with using H_{loc} . The comparison confirmed that the two cases show consistency. The left figure shows the calculation of the order parameter, and the right figure shows the difference in the order parameter for consecutive β values, in the intervals [8.33, 10], [10, 12.5], and [12.5, 16.6].

4.3 Simulation condition

The control parameters are as follows: γ represents the nonlinearity of the Josephson junction system, α represents the interaction with the external environment. The factors influencing the accuracy of the approximation method are the number of integration iterations and the size of the τ grid. We set the range of variables used in the simulation as Table 2 and Table 3.

Variables	Min	Max	Interval
γ	0	2	0.1
α	0	2	0.01
β	7.14	62.5	
Temperature	0.016	0.14	0.02 (until 0.04)

Table 2: Parameter interval used for calculation.

Number	Interval	Gridsize
τ grid	$[0, \beta]$	2000
k grid	$[0, K = 30000]$	30000

Table 3: Grid condition used for calculation.

Saturation test

We investigated the convergence behavior of the calculation results for the change of the order parameter. We were able to confirm that the results converge for the case of a tau grid size of 1800 to 2000.

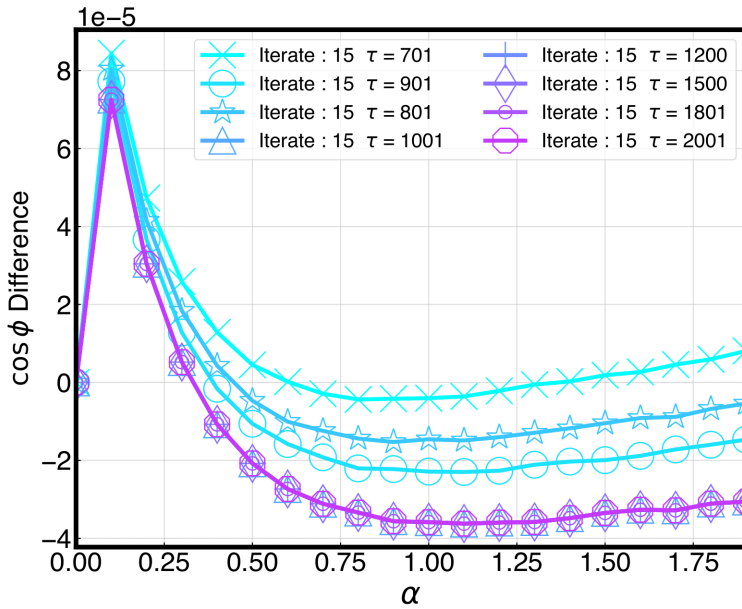


Figure 15: Saturation test in different time grid size. The temperature condition is $\beta = 41.67$

Size dependence

Since the resistively shunted Josephson junction circuit corresponds to a model that the physical system has coupled to waveguide structure, there was a breakdown of the rotating wave approximation of the two-level system as the coupling strength between the RC resonator circuit and the Josephson junction increases. The coupling strength used in this simulation is in the DSC range, including the range from the rotating wave approximation is valid to impossible.

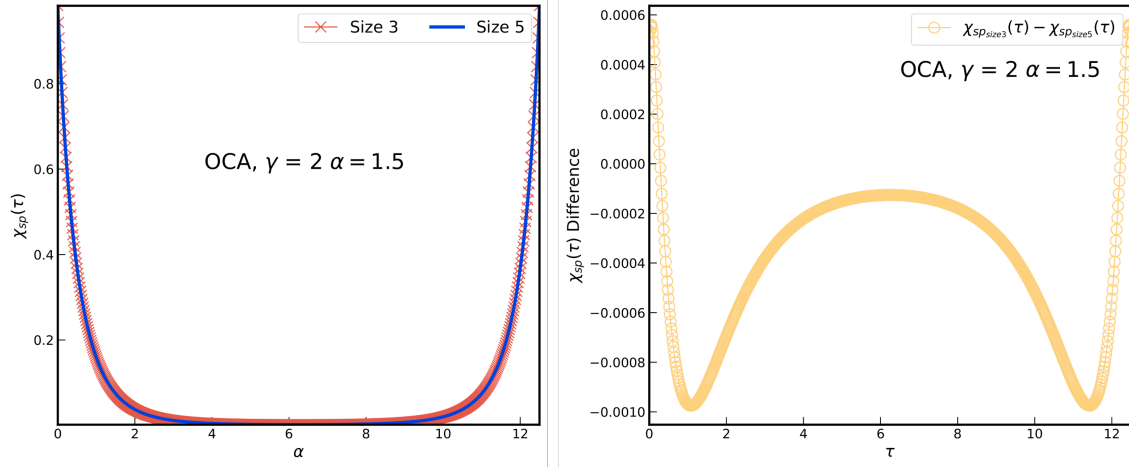


Figure 16: Comparision with $\chi_{sp}(\tau)$ size3 and size5. The size of τ grid is 700.

4.4 Orderparameter

We calculated the expectation value of the order parameter, $\cos \phi$ for various temperatures at $\alpha = 0.1$. In Figure 16, The results showed that the Josephson junction exhibits superconducting behavior as the nonlinearity increases at all temperatures. Subsequently, we examined the diagonal elements of $\cos \phi \cdot e^{H_{loc}}$ for $\alpha = 0, 0.1$, and 1. In this case, the diagonal elements represent the system being in the ground state, the even-function form of the first excited state, and the odd-function form of the first excited state, respectively. For all cases, we confirmed that the system will localized as in the ground state. This indicates that the system exhibits superconductivity, consistent with the observed expectation value of the order parameter.

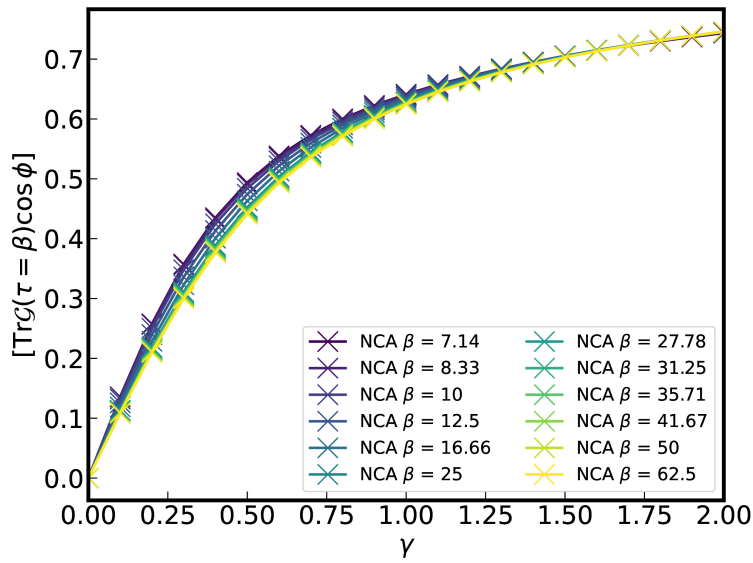


Figure 17: Result of the expectation of order parameter, $\cos \phi$.

Finite temperature criticality

To confirm the criticality of the system's phase with respect to temperature, we observed the change in the order parameter while varying the temperature. As the temperature decreases, the rate of change of the order parameter shifts from a high slope to a low slope. It can be predicted that a temperature-dependent phase transition occurs at the given point.

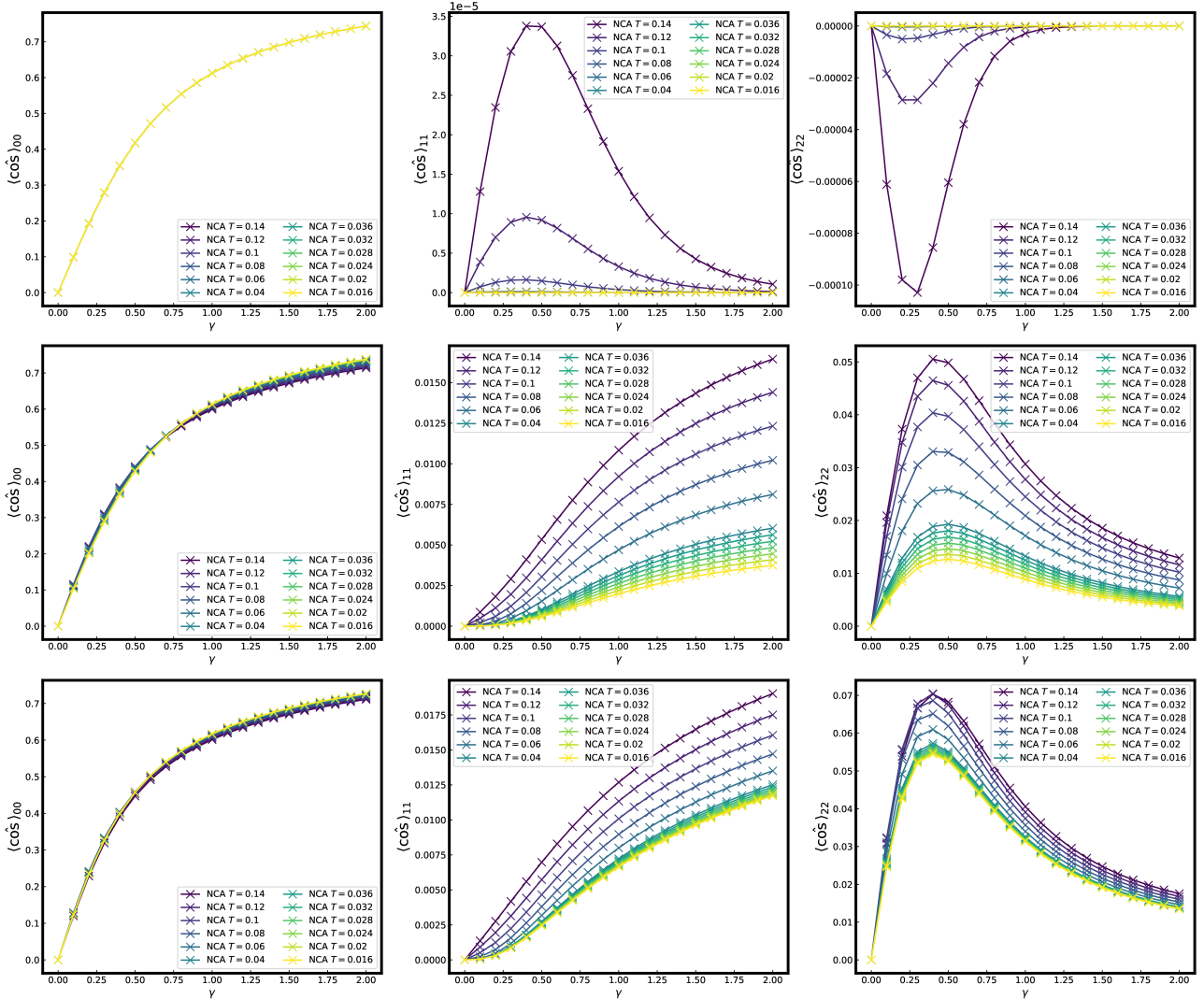


Figure 18: Change of matrix element of matrix multiplication result between $\cos \phi$ and density matrix.

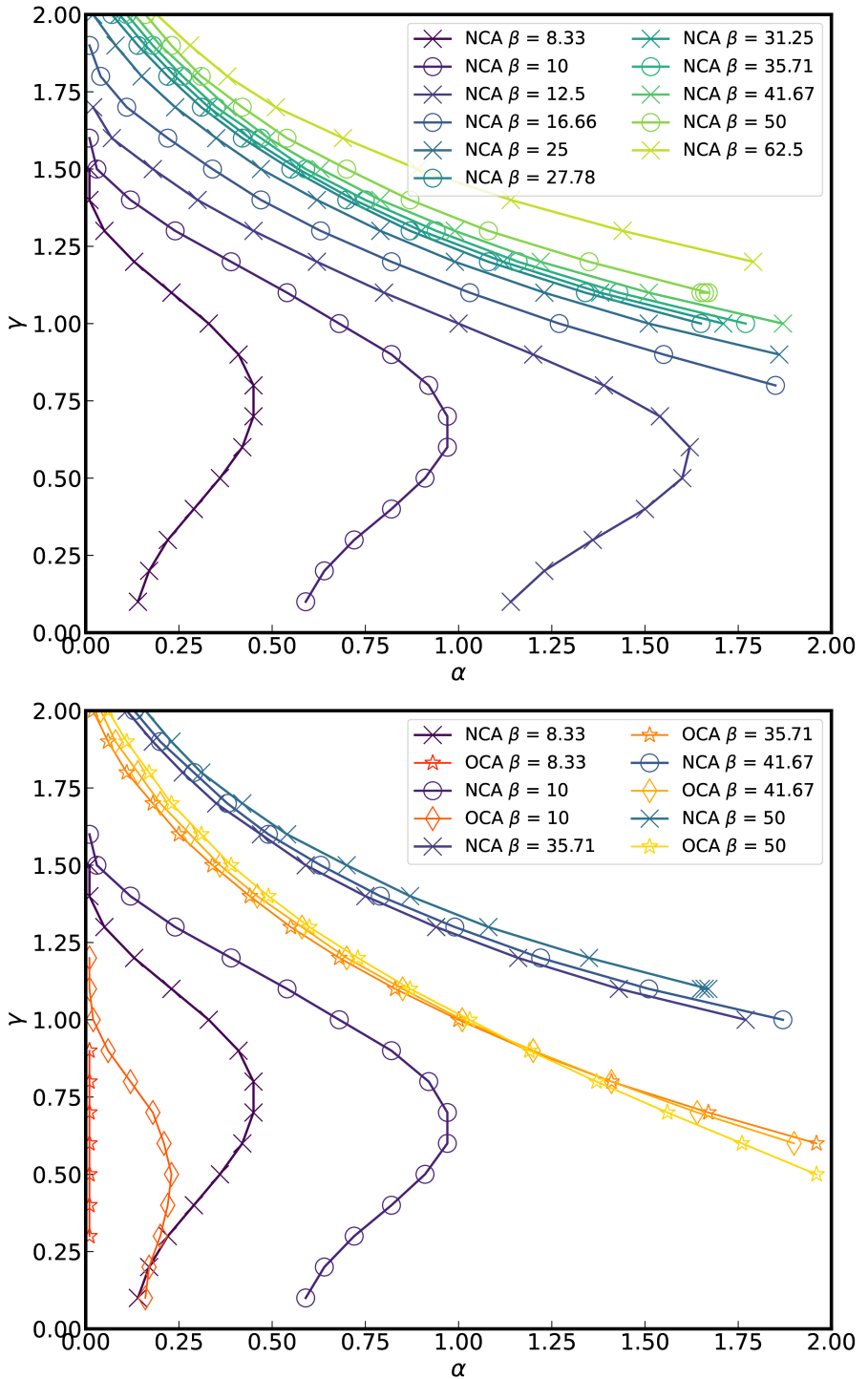


Figure 19: Figure for finite temperature criticality. Below is the comparison data between NCA and OCA.

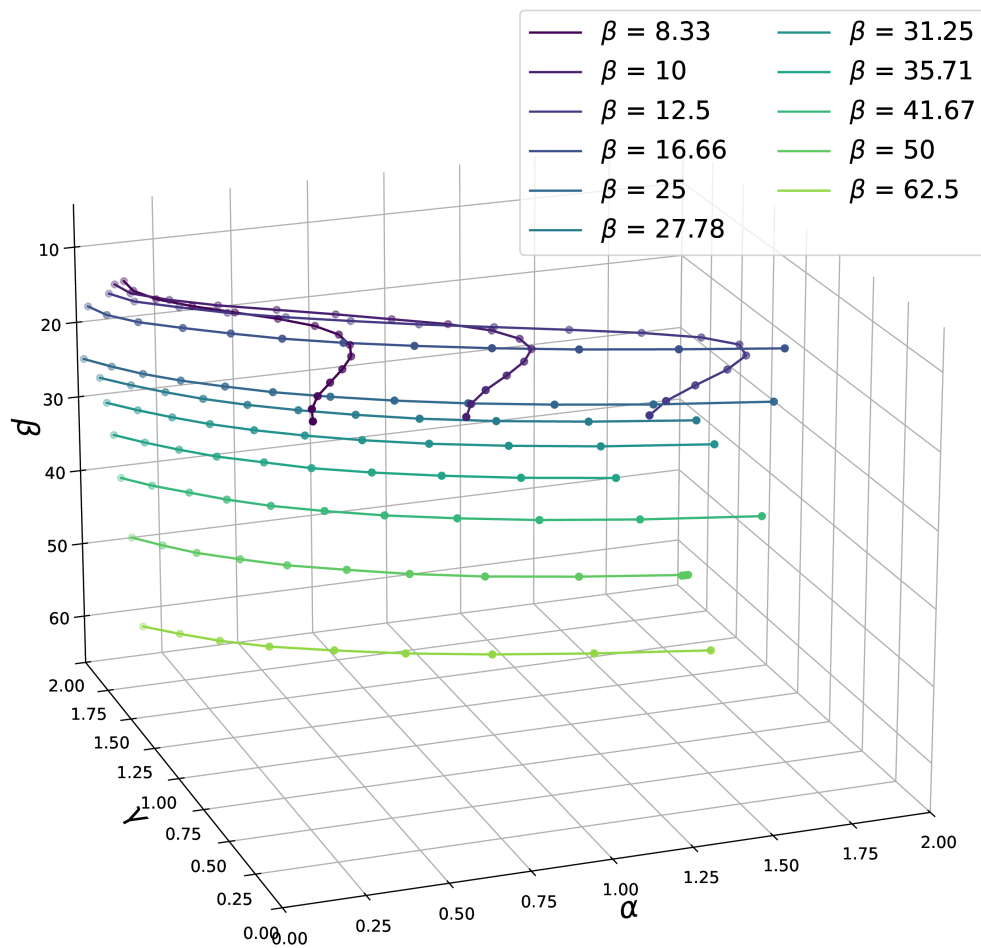


Figure 20: 3-Dimension plotting of upper Figure, Fig.17, with β axis

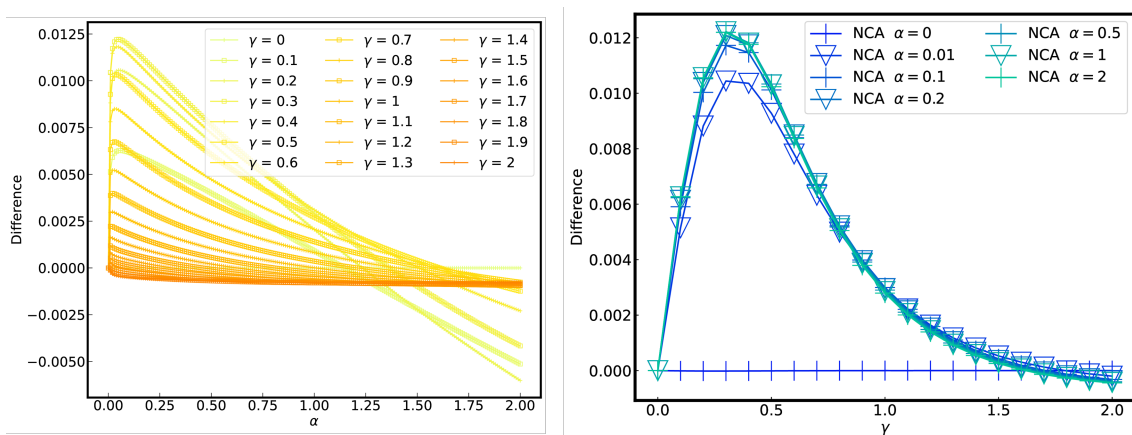


Figure 21: The crossing picture in α swapping, γ swapping

4.5 χ_{sp}

Calculating the phase transition using the relationship between the correlation function and the DC conductivity, we observed the following results: Varying the γ value at a fixed α value, conductivity tended to decrease as the interaction with the external environment increased. In particular, at low temperatures, the conductivity increased up to a certain value while the rate of change decreased with respect to the α value. When we fixed the γ value and varied the α value, the conductivity always increased at high temperatures. However, at low temperatures, we observed that the conductivity decreased as the α value increased.

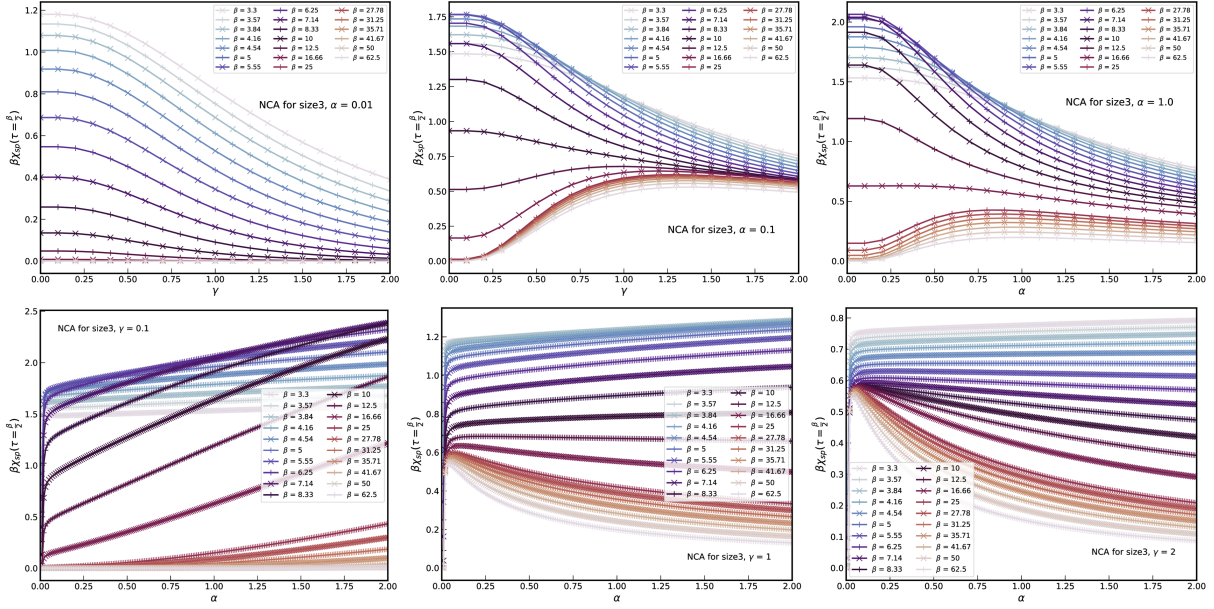


Figure 22: The crossing picture in χ_{sp} with γ swapping and α swapping

To observe how the conductivity changes for all γ and α value conditions at a fixed temperature, we visualized the results using a 2D color map. At high temperatures, we observed that the conductivity increased as the γ and α values increased. At low temperatures, the conductivity generally decreased as the influence of the external environment increased. Yet the junction energy increased, conductivity tended to increase in stronger influence from the external environment.

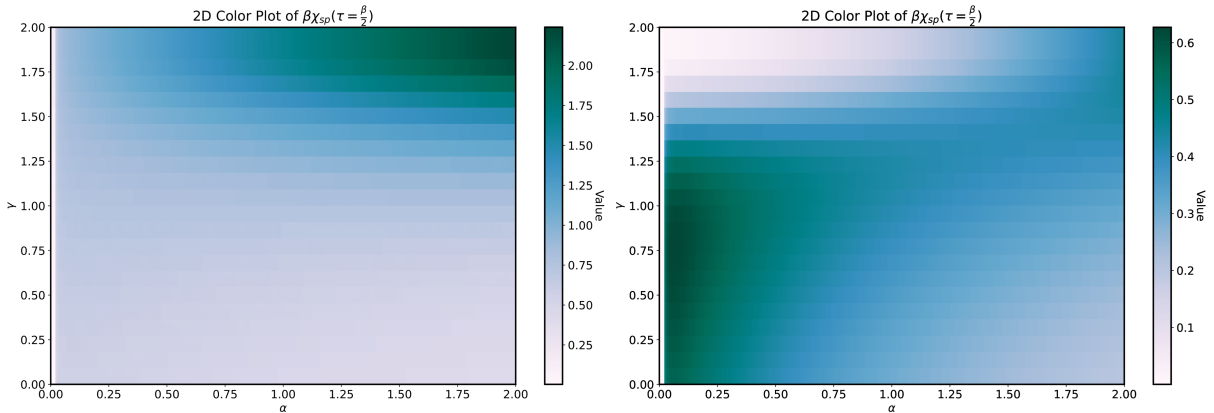


Figure 23: Colored plot for DC conductivity approximation. Left figure is in $\beta = 10$, Right is for $\beta = 25$.